Biomaterials 70 (2015) 1–11

Contents lists available at ScienceDirect

Biomaterials

journal homepage: www.elsevier.com/locate/biomaterials

A novel Trojan-horse targeting strategy to reduce the non-specific uptake of nanocarriers by non-cancerous cells

Zheyu Shen [a], Hao Wu [b], Sugeun Yang [c], Xuehua Ma [a], Zihou Li [a], Mingqian Tan [b, **], Aiguo Wu [a, *]

[a] Division of Functional Materials and Nano Devices, Ningbo Institute of Materials Technology & Engineering, Key Laboratory of Magnetic Materials and Devices, Chinese Academy of Sciences, Ningbo, Zhejiang, 315201, China
[b] Division of Biotechnology, Dalian Institute of Chemical Physics, Chinese Academy of Sciences, Dalian, 116023, China
[c] Department of New Drug Development, School of Medicine, Inha University, Incheon, 400-712, South Korea

ARTICLE INFO

Article history:
Received 8 August 2015
Accepted 9 August 2015
Available online 10 August 2015

Keywords:
Trojan-horse targeting strategy
MRI contrast agents
Active targetability to cancer cells
Non-specific uptake by non-cancerous cells

ABSTRACT

One big challenge with active targeting of nanocarriers is non-specific binding between targeting molecules and non-target moieties expressed on non-cancerous cells, which leads to non-specific uptake of nanocarriers by non-cancerous cells. Here, we propose a novel Trojan-horse targeting strategy to hide or expose the targeting molecules of nanocarriers on-demand. The non-specific uptake by non-cancerous cells can be reduced because the targeting molecules are hidden in hydrophilic polymers. The nanocarriers are still actively targetable to cancer cells because the targeting molecules can be exposed on-demand at tumor regions. Typically, Fe_3O_4 nanocrystals (FN) as magnetic resonance imaging (MRI) contrast agents were encapsulated into albumin nanoparticles (AN), and then folic acid (FA) and pH-sensitive polymers (PP) were grafted onto the surface of AN-FN to construct PP-FA-AN-FN nanoparticles. Fourier transform infrared spectroscopy (FT-IR), dynamic light scattering (DLS), transmission electron microscope (TEM) and gel permeation chromatography (GPC) results confirm successful construction of PP-FA-AN-FN. According to difference of nanoparticle-cellular uptake between pH 7.4 and 5.5, the weight ratio of conjugated PP to nanoparticle FA-AN-FN (i.e. graft density) and the molecular weight of PP (i.e. graft length) are optimized to be 1.32 and 5.7 kDa, respectively. *In vitro* studies confirm that the PP can hide ligand FA to prevent it from binding to cells with FRα at pH 7.4 and shrink to expose FA at pH 5.5. *In vivo* studies demonstrate that our Trojan-horse targeting strategy can reduce the non-specific uptake of the PP-FA-AN-FN by non-cancerous cells. Therefore, our PP-FA-AN-FN might be used as an accurately targeted MRI contrast agent.

1. Introduction

Accurate diagnosis of cancer is essential for improving the survival rate of cancer patients [1]. Magnetic resonance imaging (MRI) with a contrast agent has been widely used as a powerful tool for cancer diagnosis [2,3]. According to change of the relaxation times of water protons, MRI contrast agents can be classified into T_1-weighted contrast agents, such as gadolinium (Gd) chelates with a longitudinal relaxivity r_1, and T_2-weighted contrast agents, such as superparamagnetic iron oxide nanoparticles (SPION) having a transverse relaxivity r_2 [4]. In comparison with the traditional clinical T_1-weighted contrast agents, such as Magnevist (diethylene triamine pentaacetic acid, Gd-DTPA) and Dotarem (1,4,7,10-tetraazacyclododecane-1,4,7,10-tetraacetic acid, Gd-DOTA), SPION-based T_2-weighted contrast agents may be better due to better biocompatibility [5]. In order to improve the imaging efficiency, many interdisciplinary researchers have been interested in developing targeted SPION-based T_2-weighted contrast agents [6]. Currently, the commercial SPION-based T_2-weighted contrast agents, such as Feridex, Endorem and Resovist, are all based on passive targeting strategy, which relies on enhanced permeation and retention (EPR) effects to direct accumulation of nanocarriers at tumor sites [7–9]. General features of tumors include leaky blood vessels and poor lymphatic drainage. The nanocarriers can extravasate (escape) into the tumor tissues via the leaky vessels,

* Corresponding author.
** Corresponding author.
E-mail addresses: aiguo@nimte.ac.cn (A. Wu), mqtan@dicp.ac.cn (M. Tan).

http://dx.doi.org/10.1016/j.biomaterials.2015.08.022
0142-9612/

and the dysfunctional lymphatic drainage in tumors retains the accumulated nanocarriers [10]. However, the lack of cell-specific interactions for the internalization of nanocarriers limits the targeted efficiency [11,12]. In order to further enhance selective targetability of nanocarriers towards cancer cells, grafting targeting molecules (e.g., proteins and peptides (mainly antibodies and their fragments), nucleic acids (aptamers), small molecules (ligands)) onto the nanocarrier surfaces allows active targeting [13,14]. Muthiah et al. synthesized active targeted mannose-poly(ethylene glycol)-linked SPION for targeting to antigen-presenting cells through the specific interactions of mannose on the SPION with mannose receptor on the antigen-presenting cells in the lymph node, which was tracked by MR imaging [15]. Xie et al. explored active targeted lactoferrin-conjugated SPION as an MRI contrast agent for the detection of brain gliomas *in vivo*. Lactoferrin belongs to the transferrin family, and shares 60–80% sequence identity with transferrin, which is one of the most widely used tumor-targeted ligands because transferrin receptors overexpressed in several human carcinomas including breast, ovary and brain cancers [6]. Maeng et al. synthesized novel polymeric nanoparticles composed of poly (ethylene oxide)-trimellitic anhydride chloride-folate, doxorubicin and SPION, which showed active targetability to folate receptor-expressing tumors [16].

However, one big challenge with the active targeting is non-specific binding between the targeting molecules and non-target moieties expressed on non-cancerous cells, which leads to non-specific uptake of nanocarriers by non-cancerous cells [10].

In this study, we propose a novel Trojan-horse targeting strategy to hide or expose the targeting molecules of nanocarriers on-demand. The non-specific uptake of the nanocarriers by non-cancerous cells en route to tumor sites could be reduced because the targeting molecules are hidden in hydrophilic polymers. The nanocarriers are still active targetable to cancer cells because the targeting molecules can be exposed on-demand at tumor regions. Typically, SPION (i.e. Fe_3O_4 nanocrystals, FN) are synthesized by a polyol method and encapsulated into albumin nanospheres (AN), which are prepared by a desolvation method. A ligand folic acid (FA) and a pH-sensitive polymer (PP) are then respectively conjugated onto the surface of FN-loaded AN (AN-FN). The design of our actively targeted nanocarriers and the principle of reducing the non-specific uptake by non-cancerous cells are shown in Scheme 1. PP and FA conjugated FN-AN (PP-FA-AN-FN) can circulate in blood stream (pH ~ 7.4) with a significantly long circulation half-life for two reasons. First, the PP-FA-AN-FN cannot be recognized and captured by non-cancerous cells without folate receptor α (FRα) on the surface. Second, the hydrophilic polymer PP can prevent FA from binding to the non-cancerous cells with non-specific receptors because FA is hidden in the spreading hydrophilic polymer PP. However, the pH-sensitive polymer, whose phase transition pH is 5.0–6.0, can shrink at tumor sites resulting in exposure of the hidden FA because the pH value at tumor regions is usually more acidic (pH ~ 5.5) than blood plasma (pH ~ 7.4) [17–19]. The exposed FA can bind to cancer cells with FRα on the surface inducing cellular uptake of the PP-FA-AN-FN by FRα-mediated endocytosis. Therefore, our PP-FA-AN-FN might be used as an accurately targeted MRI contrast agent.

2. Materials and methods

2.1. Materials

N-isopropylacrylamide (NIPAM), methacrylic acid (MAA) and 2-aminoethyl methacrylate hydrochloride (AMA) monomers were purchased from Sigma–Aldrich. The NIPAM was purified by recrystallization in *n*-hexane and dried in vacuum at room temperature. Initiator *2,2′*-Azobisisobutyronitrile (AIBN) was obtained from Adamas Reagent, Ltd. (Shanghai). Chain transfer agent 2-(Dodecylthiocarbonothioylthio)-2-methylpropionic acid (DMP) was purchased from Sigma–Aldrich. Bovine Serum Albumin (BSA), 1-ethyl-3-(3-dimethylaminopropyl) carbodiimide (EDC), N-hydroxysuccinimide (NHS), L-Lysine (Lys), and 50% glutaraldehyde aqueous solution were purchased from Sigma (USA). Dulbecco's modified eagle's medium (DMEM), trypsin-EDTA, penicillin-streptomycin, fetal bovine serum (FBS) were purchased from Gibco-BRL (Grand Island, NY). *3*-(*4,5*-Dimethylthiazol-*2*-yl)-*2,5*-diphenyltetrazolium bromide (MTT) was purchased from Merck. Rhodamine phalloidine and Hoechst were purchased from Invitrogen, Carlsbad, USA. All other chemicals were analytical grades and used directly without further purification.

2.2. Copolymer synthesis

Random copolymers of NIPAM and MAA (PNIPAM-MAA), block copolymers of NIPAM, MAA and AMA (PNIPAM-MAA-*b*-AMA) were synthesized by reversible addition-fragmentation chain transfer (RAFT) polymerization using AIBN as the initiator and DMP as the chain transfer agent. Total amount of the monomers, molar ratio of the chain transfer agent DMP to the initiator AIBN, and volume of the solvent ethanol were respectively controlled at 40 mmol, 2.0 and 15 mL in all cases with more synthesis details listed in Table 1. The random copolymers of PNIPAM-MAA were synthesized by a one-step reaction. Briefly, 40 mmol of monomer mixtures, 0.25 mmol of AIBN and 0.50 mmol of DMP were dissolved in 15 mL of ethanol. The solution was degassed under reduced pressure. Polymerization was carried out at 60 °C for 24 h under nitrogen atmosphere. The block copolymers of PNIPAM-MAA-*b*-AMA were synthesized by a two-step reaction. The random copolymerization of NIPAM and MAA was first carried out at 60 °C for 16 h in the presence of nitrogen. The degassed AMA monomer (6.3 mL, 0.19 M in ethanol) was then charged to the reaction mixture. The copolymerization was further continued at the same temperature for another 8.0 h under the protection of nitrogen. The obtained copolymers were condensed and precipitated in diethylether, followed by drying in vacuum.

2.3. Synthesis of Fe_3O_4 nanocrystals-loaded albumin nanoparticles

Fe_3O_4 nanocrystals (FN) with a narrow size distribution were synthesized by a polyol method [5]. Brifely, 2.0 mL of aqueous solution of $FeCl_3 \cdot 6H_2O$ (0.375 M) and $FeCl_2 \cdot 4H_2O$ (0.45 M) was dropwise added into 100 mL of diethylene glycol (DEG) solution. The mixture was refluxed at 170 °C for 15 min and then 5.0 mL of the aqueous NaOH solution (3.0 M) was added. The temperature was kept at 170 °C for 1.0 h and then cooled to the room temperature. The obtained FN was washed with HNO_3 (1.0 M) solution and collected by a neodymium magnet.

The purified FN was then encapsulated into albumin nanoparticles (AN) via a modified desolvation method [5]. The FN dispersion (1.0 mL, 1.2 mg/mL) was mixed with BSA aqueous solution (1.0 mL, 40 mg/mL) under stirring. Ethanol (6.0 mL) was then dropwise added (2.3 mL/min). When the ethanol was running out, 60 μL of glutaraldehyde aqueous solution (8.0 wt%) was rapidly added into the mixture to crosslink the obtained nanoparticles. After 24 h, 1.0 mL of Lys (40 mg/mL) was added to cap the free aldehyde groups. After 2.0 h, the FN-loaded AN (AN-FN) were separated by centrifugation (16,000× *g*, 20 min) and washed thrice with MilliQ water. The purified AN-FN was subsequently dispersed in pure water. An aliquot of the SPION-AN dispersion was dried at 70 °C, and the concentration was calculated.

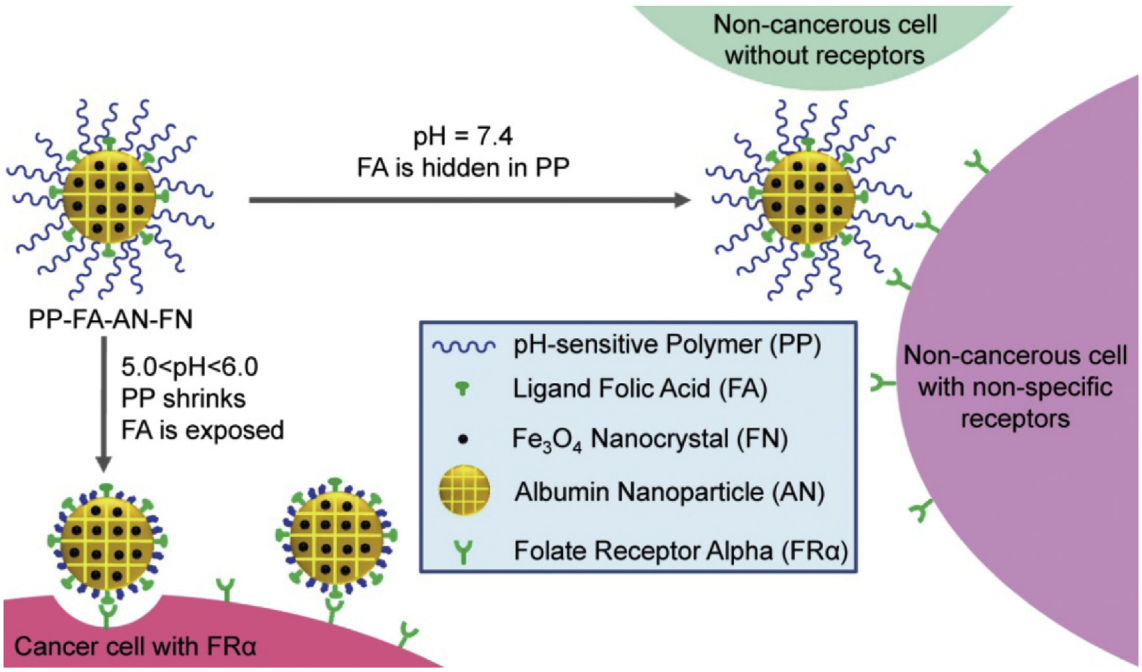

Scheme 1. Scheme of the design of our Trojan-horse targeting MRI contrast agent and the principle of reducing the non-specific uptake by non-cancerous cells. PP-FA-AN-FN cannot be recognized and captured by non-cancerous cells without FRα on the surface. The hydrophilic polymer PP can prevent FA from binding to the non-cancerous cells with non-specific receptors because FA is hidden in the spreading PP. At acidic tumor sites, the pH-sensitive polymer PP shrinks, and then the hidden FA is exposed and able to bind to cancer cells with FRα on the surface.

Table 1
Synthesis and characterization of the random copolymer PNIPAM-MAA and block copolymer PNIPAM-MAA-*b*-AMA.

Copolymer nomenclature	NIPAM (mmol)	MAA (mmol)	AMA (mmol)	[M]/[AIBN] (molar ratio)[a]	Yield (%)[b]	LCST at pH 5.5[c]	LCST at pH 7.4[c]	Mn (kDa)[d]	Mn (kDa)[e]
PNIPAM	40.0	–	–	200	78	31.9	32.0	–	–
PNIPAM-MAA1	39.6	0.4	–	200	82	33.0	33.8	–	–
PNIPAM-MAA2	39.2	0.8	–	200	89	33.8	35.0	–	–
PNIPAM-MAA3	38.8	1.2	–	200	84	34.5	36.6	–	–
PNIPAM-MAA4	38.2	1.8	–	200	83	36.1	38.9	–	–
PNIPAM-MAA5	37.6	2.4	–	200	79	36.9	39.8	–	–
PNIPAM-MAA4-*b*-AMA1	37.0	1.8	1.2	400	74	–	–	11.4	11.7
PNIPAM-MAA4-*b*-AMA2	37.0	1.8	1.2	200	80	–	–	5.7	-
PNIPAM-MAA4-*b*-AMA3	37.0	1.8	1.2	133	88	–	–	3.8	–
PNIPAM-MAA4-*b*-AMA4	37.0	1.8	1.2	100	86	–	–	2.8	1.5

[a] Molar ratio of total monomers to initiator AIBN. [DMP]/[AIBN] = 2.0.
[b] Calculated from the weight fraction of diethylether insoluble polymer to total monomers.
[c] Determined by scattered light intensity in physiological saline with increasing temperature. LCST: lower critical solution temperature.
[d] Theoretical Mn = $Mw_{monomer}$ × [M]/([DMP] + 2[AIBN]).
[e] Determined by GPC with conventional calibration.

2.4. Conjugation of folic acid onto the surface of AN-FN

Folic acid (FA) was conjugated onto the surface of SPION-AN through the reaction between −COOH of FA and $-NH_2$ of AN. EDC (20 mg) and NHS (12 mg) were added into 25 mL of ice-cooled folic acid (FA) solution (1.0 mg/mL in PBS, pH ~ 7.4) and stirred for 8.0 h at room temperature. After 8 h, 4.0 mL of the mixture was added into 76 mL of AN-FN dispersion (1.0 mg/mL in PBS, pH ~ 7.4) and then stirred at room temperature for 16 h. The resulted FA-conjugated AN-FN (FA-AN-FN) dispersion was then ultra-centrifuged (16,000× *g*, 20 min) and the supernatant was stored for further analysis. The unreacted FA remaining in the supernatant was quantified using a UV-spectrophotometer (Lambda 950, Perkin elmer, USA). The absorbance (wavelength = 363 nm) of the supernatant was converted into a FA concentration by using a calibration curve constructed with standard FA solutions. A simple mass balance was then used to calculate the FA conjugation amount on the surface of AN-FN.

2.5. Graft of pH-sensitive polymer onto the surface of FA-AN-FN

The pH-sensitive polymers (PP) were grafted onto the surface of FA-AN-FN through the reaction between −COOH of AN and $-NH_2$ of the AMA moiety in PNIPAM-MAA-*b*-AMA polymers. EDC (20 mg) was dissolved in 10 mL of AN or FA-AN-FN ice-cold dispersion (1.0 mg/mL). After that, 2.0 mL of ice-cold PNIPAM-MAA4-*b*-AMA1-4 aqueous solution (5.0–40 mg/mL) was respectively added into the above-mentioned nanoparticle dispersion. The mixture was stirred at room temperature for 16 h. The unreacted EDC and PNIPAM-MAA4-*b*-AMA were removed by washing and centrifugation (16,000× *g*, 20 min). The harvested PNIPAM-MAA-*b*-AMA-conjugated FA-AN-FN (PP-FA-AN-FN) samples were dispersed in

10 mL of MilliQ water. The nanoparticle dispersion (5.0 mL) was dried at 70 °C to calculate the concentration of PP-FA-AN-FN. The mass difference of FA-AN-FN before and after conjugating polymers was used to calculate the conjugation amounts. The preparative conditions and the results are summarized in Table 2.

2.6. Characterization of the polymers and nanoparticles

2.6.1. Determination of LCST or pH-sensitive behavior by dynamic light scattering

The scattered light intensity (derived count rate) of aqueous copolymer solutions (5.0 mg/mL) or the size distributions of the PNIPAM-MAA-*b*-AMA-conjugated albumin nanoparticle (PP-AN) dispersions (0.2 mg/mL) was measured at different temperatures or pH values by dynamic light scattering (DLS) using a Zeta Particle Size Analyser (Nano-ZS, Malvern Instrument). The data were collected on an autocorrelator with a detection angle of scattered light at 173°. The CONTIN software package was used to analyze the intensity−intensity autocorrelation functions.

2.6.2. Gel permeation chromatography measurements

Gel permeation chromatography (GPC) measurements were made on PNIPAM-MAA4-*b*-AMA1 and PNIPAM-MAA4-*b*-AMA4 in DMF at 40 °C using a HLC-8320 GPC equipment (TOSOH, Japan) with two TSK gel Super AW-H columns. The flow rate and the temperature of the column oven were set to be 0.6 mL/min and 40 °C, respectively. Elution times were converted into molecular weights using a calibration curve constructed with narrow polydispersity polystyrene standards.

2.6.3. FT-IR spectroscopic analysis

The Fourier transform infrared spectroscopy (FT-IR) spectra of the pH-sensitive polymer PNIPAM-MAA-*b*-AMA (PP), albumin nanospheres (AN, obtained from the mixture of AN and PP by washing and centrifugation), and PP-grafted AN (PP-AN, obtained from the reaction product of AN and PP by washing and centrifugation) samples in KBr discs (3 mg sample/150 mg KBr disc) were recorded using a Nicolet 6700 spectrophotometer (Thermo scientific, America) in a spectral range of 4000−400 cm^{-1}.

2.6.4. High-resolution transmission electron microscopy

To obtain detailed structural and morphological information, approximately 1 μL of the diluted nanoparticle dispersion was dropped onto a copper grid coated by a thin layer of carbon film and then dried at room temperature. Transmission electron microscope (TEM) images were recorded from a JEOL-2100 (JEOL, Japan) instrument which were operated at 200 kV.

2.7. In vitro studies

2.7.1. Cell culture

Human breast cancer cell line MCF-7 was cultured in the DMEM medium supplemented with 10 wt% fetal bovine serum (FBS), 100 units mL^{-1} of penicillin and 100 mg mL^{-1} of streptomycin. Human normal breast epithelial cell line MCF-10A was cultured in the DMEM/F12 medium supplemented with 5 wt% horse serum, 100 mg/mL EGF, 1 mg/mL hydrocortizone, 1 mg/mL cholera toxin, 10 mg/mL insulin, 100 units mL^{-1} of penicillin and 100 mg mL^{-1} of streptomycin.

2.7.2. Optimization of incubation time of PP-FA-AN-FN nanoparticles with cells

To confirm the pH-sensitive polymers (PP) could hide ligand FA to prevent it from binding to cells with FRα at pH 7.4 and shrink to expose FA at pH 5.5, we need to investigate the cellular uptake of PP-FA-AN-FN nanoparticles at pH 7.4 or 5.5 by MCF-7 cells. Because the cell growth at pH 5.5 may be worse than that at pH 7.4, we first need to study the influence of pH value on the cell growth and optimize the incubation time of cells at pH 5.5.

MCF-7 cells (100 μL) were seeded in a 96-well plate at a density of 1×10^5 cells/mL. Cells were allowed to adhere overnight at 37 °C in a humidified atmosphere containing 5% CO_2. The growth medium was replaced with 100 μL of PBS (pH ~ 5.5 or 7.4). After 1–6 h, the PBS was replaced with complete growth medium. The total incubation time of the cells was 24 h. Subsequently, 10 μL of MTT (5.0 mg/mL in PBS) was added to each well. After additional 4.0 h incubation, the growth medium was removed and 100 μL of DMSO was added in each well to dissolve the resulted formazan crystals. The automated plate reader (iMark 168-1130, Bio-rad, USA) was applied to measure the absorbance at 550 nm wavelength.

2.7.3. Analysis of the nanoparticle-cellular uptake

The quantity of the internalized nanoparticles in MCF-7 cells was measured using a steady-state fluorescence spectrophotometer (F-4600, HITACHI). 7.0 mL of cells was seeded in a cell culture dish (ϕ 90 mm × 20 mm) at a density of 5.0×10^5 cells/mL and allowed to adhere overnight. The growth medium was then replaced with 7.0 mL of nanoparticle dispersion (0.2 mg/mL, pH ~ 5.5 or 7.4). After 2.0 h incubation, the cells were washed by PBS and cultured in complete growth medium for further 24 h. Finally, the cells were washed thrice with PBS, treated with trypsin for 3.0 min and then centrifuged at 500× *g* for 5 min to remove the extracellular nanoparticles. The precipitated cells were dissolved in 3.0 mL of DMSO and subjected to fluorescent examination. The cell samples were excited at 490 nm and the fluorescence intensity at the wavelength of 530 nm was recorded. The fluorescence emission intensities were converted into the nanoparticle concentrations using a calibration curve constructed with standard concentrations

Table 2
Preparative conditions and results of PP-FA-AN-FN.

Nanoparticle nomenclature	[PP]/[FA-AN-FN] (weight ratio)[a]	PNIPAM-MAA4-*b*-AMA[b]	Conjugating amounts[c]
PP2-FA-AN-FN8	8	PNIPAM-MAA4-*b*-AMA2	1.64
PP2-FA-AN-FN4	4	PNIPAM-MAA4-*b*-AMA2	1.32
PP2-FA-AN-FN2	2	PNIPAM-MAA4-*b*-AMA2	0.74
PP2-FA-AN-FN1	1	PNIPAM-MAA4-*b*-AMA2	0.46
PP1-FA-AN-FN4	2	PNIPAM-MAA4-*b*-AMA1	1.44
PP3-FA-AN-FN4	2	PNIPAM-MAA4-*b*-AMA3	1.36
PP4-FA-AN-FN4	2	PNIPAM-MAA4-*b*-AMA4	1.28

[a] Calculated from the ratio of the feed weight of PNIPAM-MAA4-*b*-AMA (PP) to that of FA-AN-FN.
[b] The kind of copolymers used for the conjugating reaction.
[c] The weight ratio of the conjugated polymer PP to nanoparticle FA-AN-FN.

of nanoparticle dispersions.

Uptake of the nanoparticles by MCF-7 or MCF-10A cells was further studied using laser scanning confocal microscope (LSCM). The ethanol treated glass slides were put in 6-well plates. 2.0 mL of MCF-7 or MCF-10A cells in growth medium were seeded into each well at a density of 6×10^4 cells/mL and allowed to adhere at 37 °C overnight. The growth medium was then replaced with a fresh one containing FA-AN-FN or PP2-FA-AN-FN4 nanoparticles (0.20 mg/mL, pH ~ 5.5 or 7.4). After 2.0 h incubation, the cells were washed by PBS and cultured in complete growth medium for further 12 h. The cells were then washed twice with PBS, fixed with 4% formaldehyde for 30 min, permeabilized with 0.1% Triton X-100 for 5 min, blocked with 1.0% BSA for 30 min and treated with the mixture of Rhodamine phalloidine (5.0 U/mL) and Hoechst (5.0 μg/mL) for 30 min at room temperature. Finally, the samples were simultaneously excited at 405, 488 and 543 nm and the fluorescent images at emission wavelengths of 420–480, 500–540 and 600–660 nm were observed by a LSCM (TCS SP5 II, Leica, Germany).

2.7.4. In vitro MRI studies

The *in vitro* MR images of the cancer cells were observed by Siemens Avanto MRI scanner system (Siemens, Germany) with the magnetic field of 1.5 T (TR = 3000 ms, TE = 90 ms). MCF-7 cells (9.0 mL) was seeded in each culture dish (Φ 90 mm × 20 mm) at a density of 5.0×10^5 cells/mL and allowed to adhere overnight. The growth medium was replaced with 9.0 mL of FA-AN-FN or PP2-FA-AN-FN4 nanoparticle dispersion ([Fe] = 0.3 mM, pH ~ 5.5 or 7.4). After 2.0 h incubation, the cells were washed by PBS and cultured in complete growth medium for further 24 h. After that, the cells were washed thrice with PBS, treated with trypsin and centrifuged at 500× *g* for 5 min to remove the extracellular nanoparticles. The precipitated cells were resuspended in 3 mL of agrose solution (1%) in small tubes. These samples were placed in a 4 °C refrigerator until solidification for MR iamging [5].

2.8. In vivo studies

The *in vivo* MR imaging efficiency of our nanoparticles after intravenous injection (via tail vein) was further studied to confirm the positive *in vitro* results.

2.8.1. Tumor model

All animal experiments were conducted in accordance with IACUC approved protocols. Female BALB-nu/nu mice (4–6 weeks) were purchased from the Animal Center of Dalian Medical University. MCF-7 cells were inoculated by subcutaneous injection of $1.5^{*}10^7$ cells in 100 μL serum-free media and 100 μL Matrigel nearby the second breast fat pad. In vivo experiments were carried out when the size of tumor reached to around 7 mm.

2.8.2. MRI of breast cancer

Tumor-bearing mice were anesthetized by 2% isoflurane and FN, FA-AN-FN or PP-FA-AN-FN was injected at a FN dose of 20 mg/kg body weight via tail vein. T_2-weighted MRI were taken on a 0.5 T animal MRI scanner (Mini MR-60, Niumag Corporation, Shanghai, China) before injection (0 min) and after injection (20 min, 24 h, 48 h, 72 h). T_2-weighted images were acquired using the following parameters: TR = 2500 ms; TE = 50 ms; slice thickness = 2.5 mm; slice spacing = 0.5 mm; FOV 100 mm * 100 mm, average = 3. All the animal experiments were performed on the same mice (BALB-nu/nu mice).

2.9. Statistical analysis

Statistical significance was determined by application of Student's *t*-test or by a one-way ANOVA followed by Student-Newman-Keuls test using Sigma Stat version 3.5. The significance level was fixed as $P < 0.05$.

3. Results and discussion

3.1. Synthesis and characterization of polymers

We first followed a reported method, i.e. reversible addition-fragmentation chain transfer (RAFT) polymerization [20,21], to synthesize pH-sensitive polymers. Poly(*N*-isopropylacrylamide-*co*-methacrylic acid) (PNIPAM-MAA) and poly(*N*-isopropylacrylamide-*co*-methacrylic acid-*b*-2-aminoethyl methacrylate hydrochloride) (PNIPAM-MAA-*b*-AMA) are synthesized by the RAFT polymerization using *2,2′*-Azobisisobutyronitrile (AIBN) as the initiator and 2-(Dodecylthiocarbonothioylthio)-2-methylpropionic acid (DMP) as the chain transfer agent (Scheme 2). The details of synthesis and characterization are summarized in Table 1. After copolymerization, the procedure of non-solvent precipitation and vacuum drying are used to eliminate the residual of un-reacted monomers and solvents. For all these copolymers, the yield and conversion are found to be above 74%.

Poly(methacrylic acid) (PMAA) is an ionizable hydrophilic polymer, which is pH-sensitive due to the ionization/deionization of the −COOH. At high pH values, the linear PMAA keeps at spreading state because the −COOH groups are ionized and the charged −COOH groups repel each other. At low pH values, the PMAA keeps at shrunk and collapsed state since the −COOH groups are not ionized [22,23]. Poly(N-isopropylacrylamide) (PNIPAM) is a well-known temperature-sensitive polymer which exhibits drastic phase transition at its lower critical solution temperature (LCST) of 32 °C [24–26]. One of the objectives of this work is to synthesize the pH- and temperature-sensitive copolymers of NIPMA and MAA (PNIPAM-MAA), to investigate the pH- and temperature-sensitive behavior under various pH and temperature conditions.

Dynamic light scattering (DLS) results show the pH- and temperature-sensitive behavior of the synthesized PNIPAM-MAA (Fig. 1). The average count rates are independent of temperatures at low temperatures, which indicates no aggregate forms in solution. Beyond typical high temperatures, the count rates rapidly increase with temperature due to the phase separation of copolymer in the solutions. The coil-globule transition of single polymer chains, which results in the decrease in particle size, is not observed in Fig. 1A–F because the decrease in size due to polymer chain conformation change is negligible compared to the increase in size due to chain aggregation [27]. The LCST from the light scattering study is defined as the temperature at which the steepest slope is located as shown in Fig. 1A–F. The obtained LCSTs of PNIPAM-MAA1-5 at pH 5.5 or 7.4 are listed in Table 1, and plotted as a function of molar fraction of MAA (Fig. 1G). When the molar fraction of MAA is 0.045, the LCST of PNIPAM-MAA4 is 38.9 °C at pH 7.4 and 36.1 °C at pH 5.5, which means the PNIPAM-MAA4 shows linear coil state at 37 °C and pH 7.4, but shrinks at 37 °C and pH 5.5. The pH sensitive behavior of the PNIPAM-MAA4 at 37 °C is further investigated by DLS (Fig. 1H). The average count rates are very low when pH is above 6.5, but dramatically increase with decreasing of pH value from 6.5 and ceases to increase at pH 5.2. Because the steepest slope is located at pH 6.0 in Fig. 1H, the phase transition pH is determined to be 6.0, which meets the requirement for the above-mentioned drug delivery scheme (Scheme 1). Therefore, the molar fraction of MAA is fixed at 0.045 for the following experiments.

The PNIPAM-MAA-*b*-AMA polymers with different molecular weight, which was controlled by the molar ratio of total monomers to initiator (i.e. [M]/[AIBN]), were further synthesized by RAFT polymerization. The $-NH_2$ in AMA is used to graft the polymers

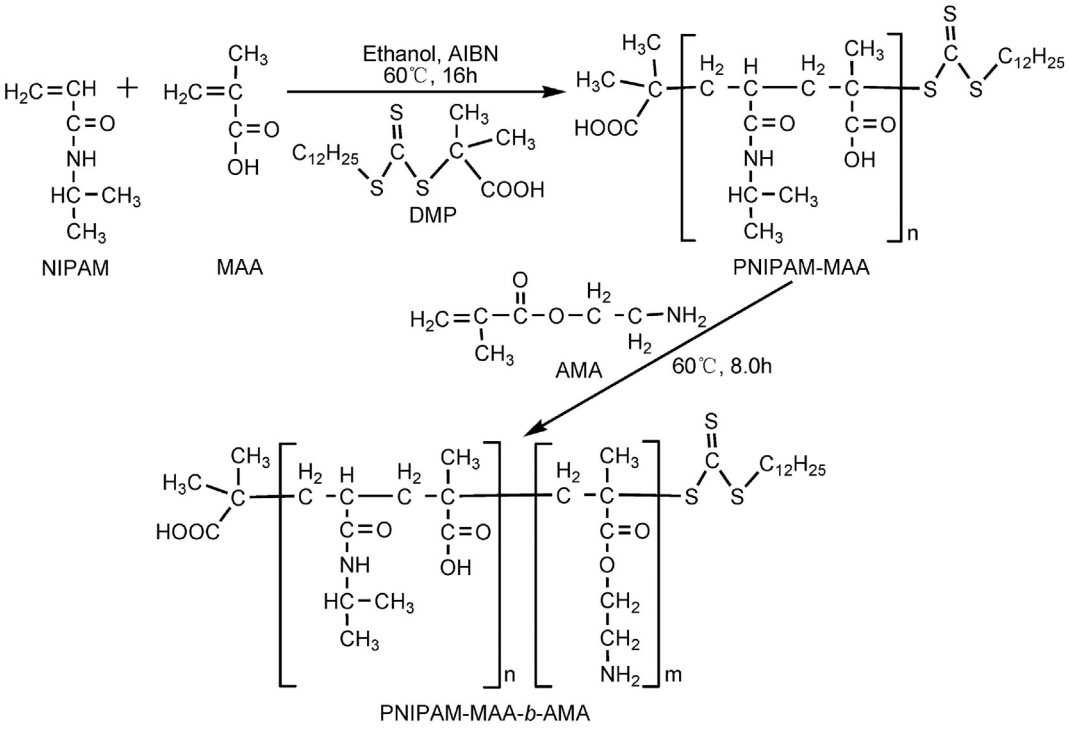

Scheme 2. RAFT copolymerization of NIPAM, MAA and AMA.

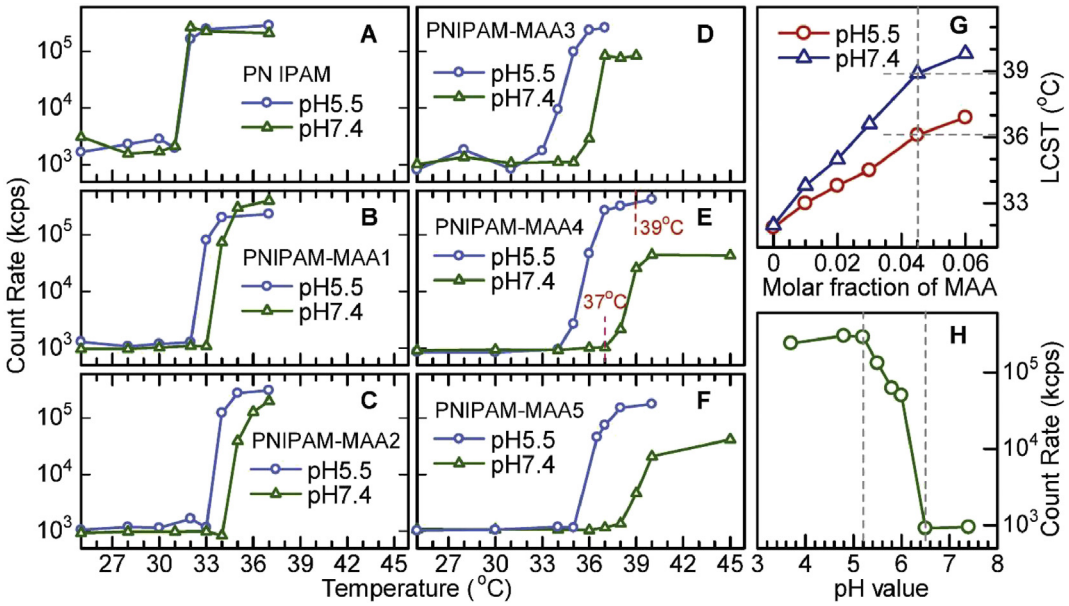

Fig. 1. The pH- and temperature-sensitive behavior of the synthesized polymers. (A–F) The count rates of PNIPAM and PNIPAM-MAA1-5 solutions (5.0 mg/mL in physiological saline, pH = 5.5 or 7.4) determined at different temperatures by DLS. (G) LCST of the PNIPAM-MAA copolymers in physiological saline (5.0 mg/mL) at pH 5.5 or 7.4 as a function of molar fraction of MAA to total monomers. (H) The count rates of PNIPAM-MAA4 solutions (5.0 mg/mL in physiological saline) at different pH values determined by DLS; the temperature and equilibrating time are respectively set to be 37 °C and 6.0 min before measurement.

onto the surface of nanoparticles. The theoretical and determined number average molecular weights (Mn) are summarized in Table 1. Because the polymers are synthesized by RAFT, the molecular weight distributions are very narrow, which can be observed from the GPC traces (Fig. S1).

3.2. Synthesis and characterization of FA-AN-FN nanoparticles

The actively targeted FA-AN-FN nanoparticles, i.e. FA-conjugated and FN-loaded AN, were prepared and characterized according to our previous report [5]. The amount of conjugated FA calculated from the weight ratio of FA to FA-AN-FN was determined to be 0.85%, and the drug loading content (DLC) of FN calculated from the weight ratio of loaded FN to FA-AN-FN was determined to be 6.0% [5]. The longitudinal relaxivity (r_1), transverse relaxivity (r_2) and r_2/r_1 ratio were respectively determined to be 1.7 mM^{-1} s^{-1}, 69.7 mM^{-1} s^{-1} and 39.6 [5]. The high r_2/r_1 ratio compared with that of the commercial Resovist® ($r_2/r_1 = 11.4$) [28] indicates the FA-AN-FN nanoparticles have a stronger T_2 shortening effect and are feasible to be used as T_2-weighted MRI contrast agents.

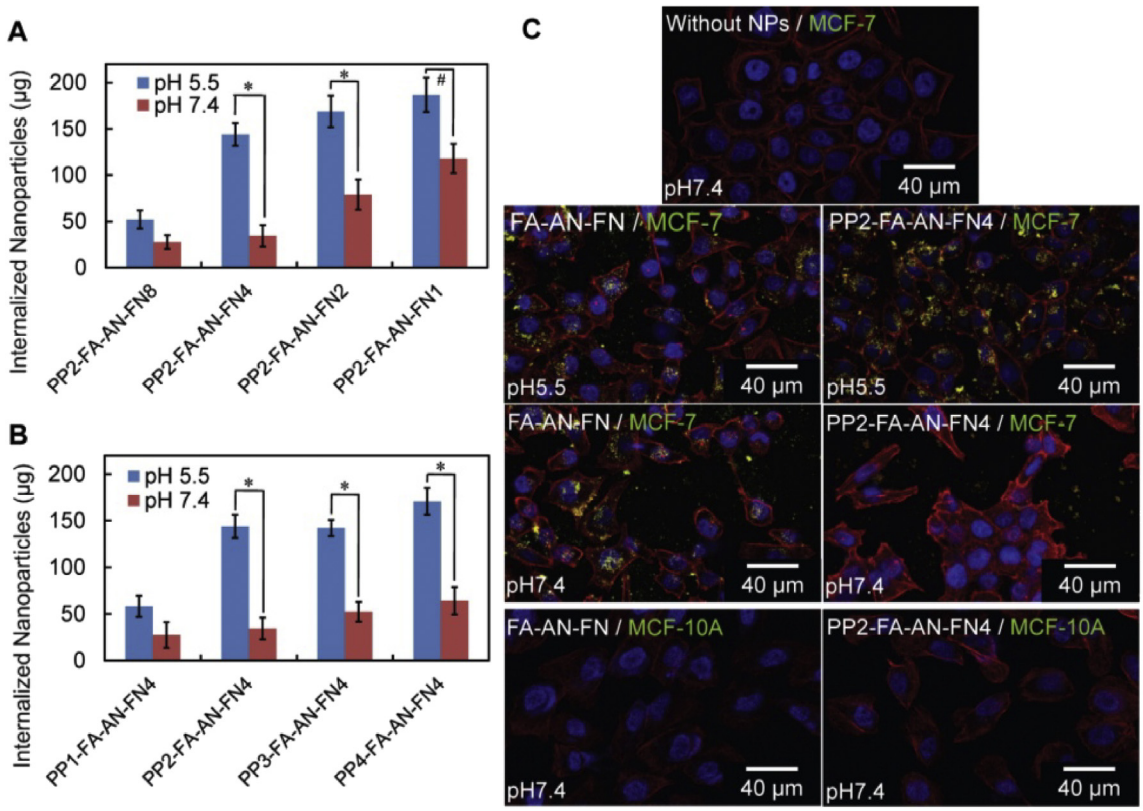

Fig. 2. Internalization of the nanoparticles by cells. (A&B) Quantification of the internalized nanoparticles by MCF-7 cells analyzed by fluorescence spectrophotometer (Mean ± SD, n = 3). (A) Influence of the graft density of the polymers on the nanoparticle-cellular uptake by MCF-7 cells. (B) Influence of the graft length (molecular weight) of the polymers on the nanoparticle-cellular uptake by MCF-7 cells. #P < 0.05, *P < 0.01. (C) The LSCM images of MCF-7 or MCF-10A cells incubated with FA-AN-FN or PP2-FA-AN-FN4 nanoparticles at pH 5.5 or 7.4. The samples were simultaneously excited at 405, 488 and 543 nm. The cytoskeleton stained with Rhodamine Phalloidin (EX 543 nm, EM 600–660 nm) is red and the nucleus stained with Hoechst (EX 405 nm, EM 420–480 nm) is blue. The fluorescent images of autofluorescent FA-AN-FN and PP2-FA-AN-FN4 are green (EM 500–540 nm) at an excitation of 488 nm, and are red (EM 600–660 nm) at an excitation of 543 nm. As such, the yellow-colored nanoparticles are associated with the combination of green and red fluorescence emissions. (For interpretation of the references to color in this figure legend, the reader is referred to the web version of this article.)

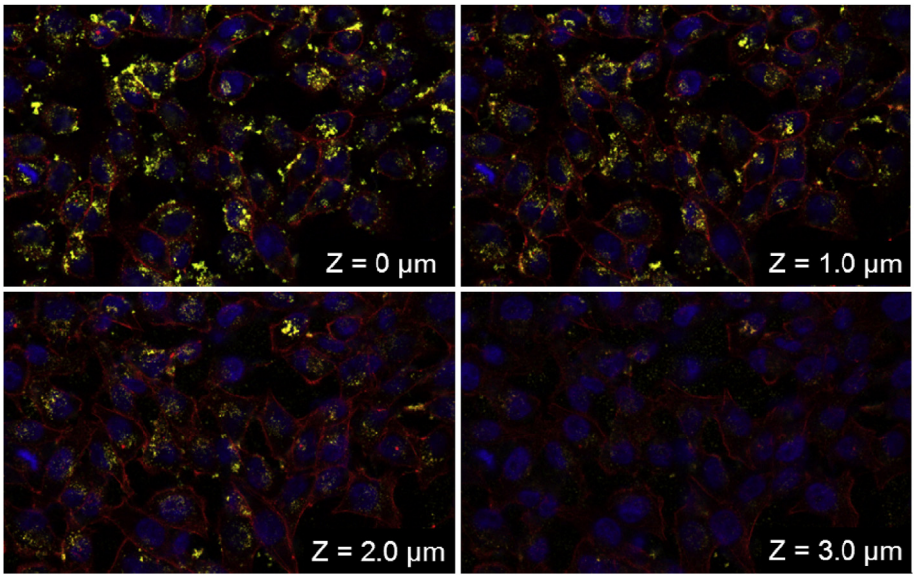

Fig. 3. XY-Z series of the LSCM images for MCF-7 cells scanned upwardly from slide glass with 1.0 μm interval. The MCF-7 cells were incubated with PP2-FA-AN-FN4 nanoparticles at pH 5.5 for 2.0 h. The actin of the cells was stained with Rhodamine Phalloidin. The nucleus was stained with Hoechst. The samples were simultaneously excited at 405, 488 and 543 nm and the fluorescent images at emission wavelengths of 420–480, 500–540 and 600–660 nm were respectively taken by LSCM. The concentrations of FA-AN-FN and PP2-FA-AN-FN4 nanoparticles in the cultured medium are 0.20 mg/mL.

3.3. Synthesis and characterization of PP-FA-AN-FN nanoparticles

To reduce the non-specific uptake of the FA-AN-FN nanoparticles by non-cancerous cells, in this study, pH-sensitive polymers were grafted onto the surface of the FA-AN-FN nanoparticles to hide the targeting molecules (Scheme 1). To verify the pH-sensitive behavior of PNIPAM-MAA4 on the surface of nanoparticles, the pH-sensitive PNIPAM-MAA4-*b*-AMA2 (PP2) was grafted onto the AN. In the FT-IR spectra (Fig. S2), AN, PP2 and PP2-grafted AN (PP2-AN) have peaks at ~1140 cm^{-1} (C—O stretching vibration), ~1650 cm^{-1} (C═O stretching vibration), ~3300 cm^{-1} (O—H stretching vibration), ~3430 cm^{-1} (N—H stretching vibration). All these peaks can be attributed to the material albumin or PNIPAM-MAA4-*b*-AMA2. Moreover, it's obvious that two characteristic peaks arise at ~880 and 930 cm^{-1} (C═S stretching vibration) [29] in the spectrum of PP2 or PP2-AN, but not in that of AN. This result demonstrates that PP2 has been successfully grafted onto the surface of AN.

The pH-sensitive behavior of PP2-AN is compared to that of AN (control) as shown in Fig. S3. The size distributions of PP2-AN in water with different pH values determined by DLS are all very narrow (Fig. S3A). With increasing pH value, the hydrodynamic diameter (d_h) of PP2-AN increases rapidly at pH 6.0, but the d_h change of AN is almost negligible (Fig. S3B). This result indicates that the pH-sensitive behavior of PNIPAM-MAA4 on the surface of nanoparticles should be similar with that of the free PNIPAM-MAA4, whose phase transition pH is determined to be 6.0 (Fig. 1H). In addition, the d_h of the nanoparticles at any pH values is smaller than 170 nm (Fig. S3), which is small enough for the endocytosis and EPR effect (extravasating into the tumor tissues via the leaky vessels) [10].

The pH-sensitive PNIPAM-MAA4-*b*-AMA1-4 (PP1-4) were grafted onto the surface of FA-AN-FN with different density (i.e. graft amount) and length (i.e. molecular weight). The preparative conditions and results of PP-FA-AN-FN are summarized in Table 2. Fig. S4 shows the TEM images of AN, AN-FN and PP2-FA-AN-FN4. The FN inside AN-FN is almost invisible in Fig. S4B because the contrast between FN and AN is very close. It could be visible in the enlarged image as shown in Fig. S4D. It is obvious that the FA and PNIPAM-MAA-*b*-AMA on the surface of AN are both not visible by TEM due to the low molecular weights [30,31]. In addition, the hydrodynamic diameter of PP2-FA-AN-FN4 in cell medium (DMEM) was measured at different temperatures from 25 to 45 °C (Fig. S5a and b). It is found that the size decreased sharply at 38 °C due to the shrinking of PNIPAM-MAA and increased rapidly when the temperature is higher than 41 °C. That's because the physicochemical properties of the particles can change in different media and this can lead in particular to agglomeration [32]. In order to reconfirm the phase transition of PNIPAM-MAA in DMEM, the count rates of PNIPAM-MAA4 in DMEM (5.0 mg/mL, pH = 7.4) is determined at different temperatures by DLS (Fig. S5c). The count rates increase rapidly when temperature is higher than 38 °C, which is similar with the behavior of PNIPAM-MAA in saline (Fig. 1E).

3.4. Optimization of incubation time of cells at pH 5.5

Fig. S6 shows the influence of the pH value of PBS that was incubated with the MCF-7 cells for different times on the cell growth. The cell viabilities at pH 5.5 are much lower than those at pH 7.4 when the incubation time is longer than 3.0 h, but they are comparable when incubation time is shorter than 2.0 h. That's because short exposure time (≤2 h) with PBS and followed up with long incubation time (24 h) with regular medium may significantly decrease any differences caused by pH difference. The incubation time of PP-FA-AN-FN nanoparticles at pH 7.4 or 5.5 with cells in the following experiments is fixed at 2.0 h due to the similar cell growth between pH 7.4 and 5.5.

3.5. Optimization of graft density and length of polymers on ther surface of PP-FA-AN-FN

To check whether the pH-sensitive polymers (PP) could hide ligand FA to prevent it from binding to cells with FRα at pH 7.4 and shrink to expose FA at pH 5.5, we investigated the cellular uptake of PP-FA-AN-FN by MCF-7 cells at pH 7.4 or 5.5. The fluorescence emission intensities of the internalized nanoparticles in cells were converted into the nanoparticle concentrations using calibration curves constructed with standard concentrations of nanoparticle dispersions (Fig. S7).

It is found that the graft density and length of pH-sensitive polymers (PP) do influence the cellular uptake of PP-FA-AN-FN by MCF-7 cells (Fig. 2). The weight ratio of the conjugated polymer PP2 to nanoparticle FA-AN-FN (i.e. graft density) is 1.64, 1.32, 0.74 and 0.46 for PP2-FA-AN-FN8, PP2-FA-AN-FN4, PP2-FA-AN-FN2 and PP2-FA-AN-FN1, respectively (Table 2). When the graft density is

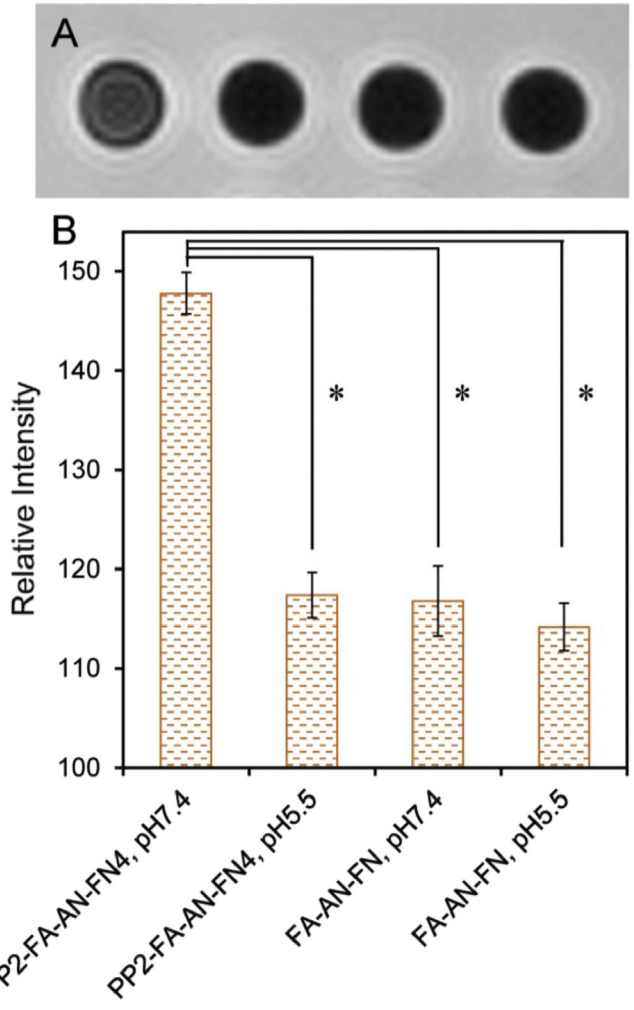

Fig. 4. *In vitro* MR images of the cancer cells. (A) T_2-weighted MR images of MCF-7 cells incubated with as-prepared nanoparticles at different pH values for 2.0 h (TR = 3000 ms, TE = 90 ms). From left to right, the samples are MCF-7 cells incubated with PP2-FA-AN-FN4 at pH 7.4, PP2-FA-AN-FN4 at pH 5.5, FA-AN-FN at p H7.4 and FA-AN-FN at pH 5.5, respectively. (B) The relative intensities of the T_2-weighted MR images of MCF-7 cells incubated with as-prepared nanoparticles at different pH values for 2.0 h (Mean ± SE). *P < 0.01.

1.64, the amount of the internalized nanoparticles by cells at pH 7.4 is comparable to that at pH 5.5. However, when the graft density is 1.32, 0.74, or 0.46, the amounts of the internalized nanoparticles by cells at pH 5.5 are much higher than those at 7.4 (Fig. 2A). That's because the ligand FA is hidden in the spreading hydrophilic polymer PP at pH 7.4, but is exposed to recognize FRα of cells after shrinking of PP at pH 5.5 (Scheme 1). The graft density is fixed at 1.32 for the following study due to the biggest difference of nanoparticle-cellular uptake between pH 7.4 and 5.5.

The molecular weight of PP1, PP2, PP3 and PP4 (i.e. graft length) is respectively 11.4, 5.7, 3.8 and 2.8 kDa (Table 1). When the graft length is 11.4 kDa, the amount of the internalized nanoparticles by cells at pH 7.4 is comparable to that at pH 5.5. However, when the graft length is 5.7, 3.8 or 2.8 kDa, the amounts of the internalized nanoparticles by cells at pH 5.5 are much higher than those at 7.4 (Fig. 2B). Because of the biggest difference of nanoparticle-cellular uptake between pH 7.4 and 5.5, the graft length is fixed at 5.7 kDa for the subsequent experiments as an optimized value. The polymers on the surface of nanoparticles cannot be too dense or too long because the shrunk polymers may also hide the targeted molecules.

3.6. Cellular uptake of the nanoparticles at pH 7.4 or 5.5 by cells

To further confirm the pH-sensitive polymers (PP) could hide ligand FA to prevent it from binding to cells with FRα at pH 7.4 and shrink to expose FA at pH 5.5, we investigated the cellular uptake of FA-AN-FN or PP2-FA-AN-FN4 nanoparticles at pH 7.4 or 5.5 by MCF-7 cells. Regarding FA-AN-FN at pH 5.5, FA-AN-FN at pH 7.4 and PP2-FA-AN-FN4 at pH 5.5, many nanoparticles are internalized into the MCF-7 cells. However, very few PP2-FA-AN-FN4 nanoparticles at pH 7.4 are incorporated in the MCF-7 cells (Fig. 2C). The different amount of nanoparticles inside the cells in the XY-Z series of LSCM images indicates that the nanoparticles do have been internalized into the cells rather than absorbed on cell surfaces (Fig. 3). Moreover, we almost cannot find any FA-AN-FN or PP2-FA-AN-FN4 nanoparticles are incorporated in the MCF-10A cells (Fig. 2C) because very few FRα is expressed on the surface of MCF-10A cells [33,34]. These results confirm the hypothesis that the non-specific uptake of actively targeted nanocarriers by non-cancerous cells (pH 7.4) could be reduced by hiding the targeting molecules in pH-sensitive polymers, which could shrink and expose the targeting molecules at tumor sites (pH ~ 5.5).

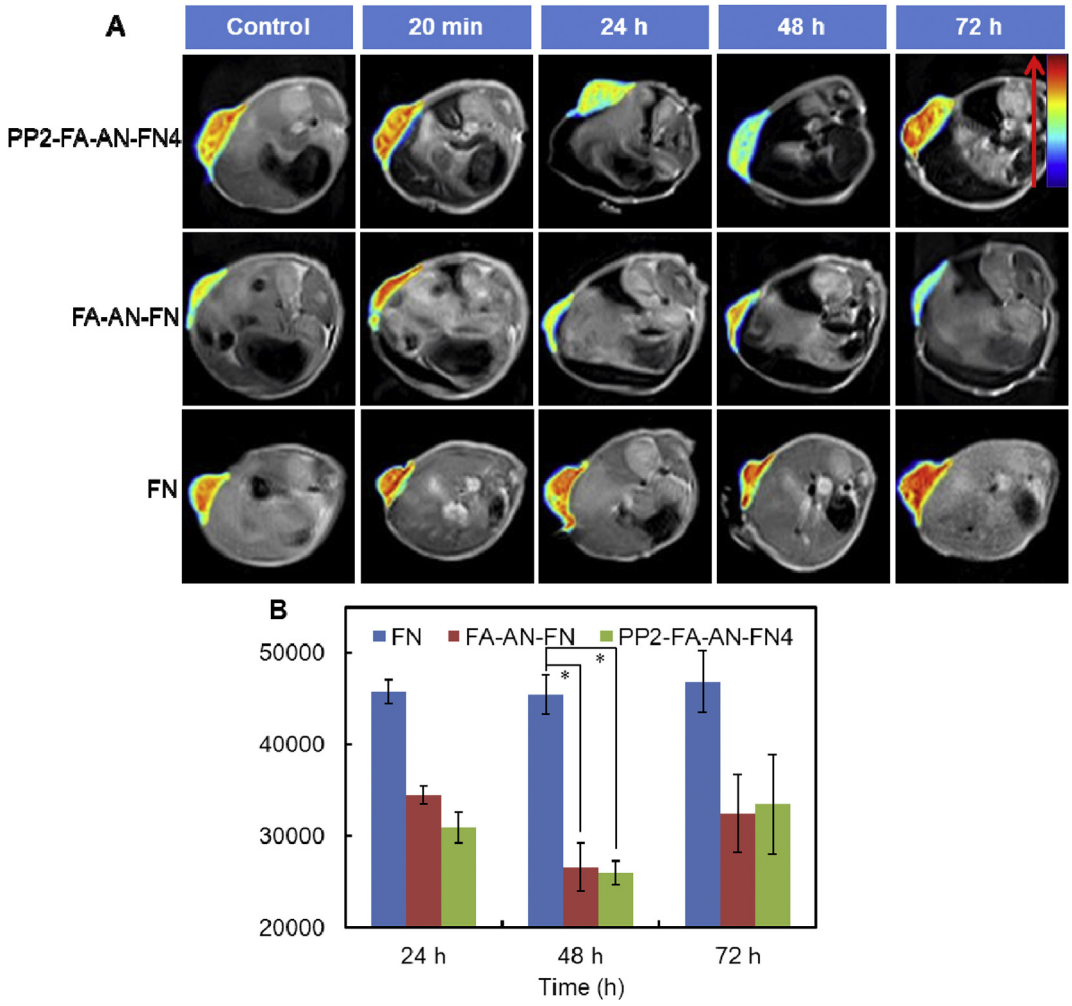

Fig. 5. In vivo MR imaging. (A) MR images of mice injected (via tail vein) with FN, FA-AN-FN or PP-FA-AN-FN at a FN dose of 20 mg/kg body weight recorded at different time points post-injection. (B) The relative intensities of T_2 signals at tumor sites measured from MR images shown in (A). *P < 0.01. All the animal experiments were performed on the same mice (BALB-nu/nu mice).

3.7. In vitro MR imaging

In order to confirm the MRI efficiency of our PP-FA-AN-FN nanoparticles, *in vitro* MR imaging is applied on the cancer cells after incubation with the nanoparticles. Fig. 4A shows T_2-weighted MR images of MCF-7 cells incubated with as-prepared nanoparticles at different pH values and Fig. 4B shows the relative intensity of the above-mentioned T_2-weighted MR images. It is obvious that the T_2-weighted images of MCF-7 cells incubated with PP2-FA-AN-FN4 at pH 5.5, FA-AN-FN at pH 7.4 and FA-AN-FN at pH 5.5 are significantly darker than that of MCF-7 cells incubated with PP2-FA-AN-FN4 at pH 7.4. These results indicate that the pH-sensitive polymer PP2 can hide or expose the targeting molecules of PP2-FA-AN-FN4 nanoparticles at pH 7.4 or pH 5.5.

The MR images (T_2 weighted) of PP2-FA-AN-FN4 nanoparticle dispersion at 1.0 mg Fe/mL are compared with those of the commercial Resovist® (Fig. S8). It is found that the contrast effect of our PP2-FA-AN-FN4 is comparable to that of the commercial Resovist®, which renders it particularly suitable to be used as a negative MRI contrast agent in T_2-weighted imaging.

3.8. In vivo MR imaging

Encouraged by the positive results of the *in vitro* MR imaging applied on the MCF-7 cells after incubation with the nanoparticles, we next studied the *in vivo* MR imaging efficiency of our nanoparticles after intravenous injection (via tail vein).

Fig. 5A shows MR images of tumor-bearing mice injected with FN, FA-AN-FN or PP2-FA-AN-FN4 at a FN dose of 20 mg/kg body weight recorded at different time points post-injection. It is found that the T_2 signals of the tumor sites are comparable to each other at different time points post-injection for FN because it lacks active targetability. However, the T_2 signals of the tumor sites decrease significantly for FA-AN-FN and PP2-FA-AN-FN4 at 24–72 h post-injection. This result indicates that our FA-AN-FN and PP2-FA-AN-FN4 are both actively targetable to the tumors due to the targeting molecule FA. Fig. 5B shows the relative intensities of T_2 signals at tumor sites measured from the MR images. It can be seen that the intensities of T_2 signals reach to maximum values for FA-AN-FN and PP2-FA-AN-FN4 at 48 h. The T_2 signal of FA-AN-FN is lower than that of FN (*$P < 0.01$) due to the active targetability of FA. In addition, the T_2 signal of PP2-FA-AN-FN4 is lower than that of FA-AN-FN and much lower than that of FN (*$P < 0.01$). This result demonstrates that the graft of PP can reduce the non-specific uptake of the nanoparticles by non-cancerous cells and thus enhance the MR imaging efficiency in the tumors.

In addition, biocompatibility of the polymers should be considered. PNIPAM showed no toxicity in mice according to a toxicity test of the PNIPAM, which was performed in comparison with that of the NIPAM monomer [30,35]. Therefore, although NIPAM, MAA and AMA are toxic monomers, PNIPAM-MAA-AMA is non-toxic and may be removed from the body due to relatively low molecular weight.

4. Conclusions

In summary, we have designed and synthesized a novel Trojan-horse targeting nanocarrier, which could reduce the non-specific uptake by non-cancerous cells. The FN as a MRI contrast agent is encapsulated into AN, and then a ligand FA and a pH-sensitive polymer PP are respectively conjugated onto the surface of AN-FN to construct PP-FA-AN-FN composite nanoparticles. The FT-IR, DLS, TEM and GPC results confirm the successful construction of PP-FA-AN-FN nanoparticles. According to the difference of nanoparticle-cellular uptake between pH 7.4 and 5.5, the graft density and graft length of PP are optimized to be 1.32 and 5.7 kDa, respectively. The *in vitro* studies confirm that the PP can hide ligand FA to prevent it from binding to cells with FRα at pH 7.4 and shrink to expose FA at pH 5.5. The *in vivo* studies demonstrate that our Trojan-horse targeting strategy can reduce the non-specific uptake of the nanocarriers by non-cancerous cells and our PP-FA-AN-FN might be used as an accurately targeted MRI contrast agent.

Acknowledgments

This work was financially supported by National Natural Science Foundation of China (Grant Nos. 51203175, 51411140243, U1432114, and 91227126), Zhejiang Provincial Natural Science Foundation of China (Grants No. LQ13E030004), the Hundred Talents Program of Chinese Academy of Sciences (2010-735), Key Breakthrough Program of Chinese Academy of Sciences (KGZD-EW-T06), the program for Ningbo Municipal Science and Technology Innovative Research Team (Grant No. 2015B11002) and National Research Foundation of Korea (NRF-2014K2A2A2000720).

Appendix A. Supplementary data

Supplementary data related to this article can be found at http://dx.doi.org/10.1016/j.biomaterials.2015.08.022.

References

[1] R. Weissleder, Molecular imaging in cancer, Science 312 (2006) 1168–1171.
[2] H. Yim, S.G. Yang, Y.S. Jeon, I.S. Park, M. Kim, D.H. Lee, Y.H. Bae, K. Na, The performance of gadolinium diethylene triamine pentaacetate-pullulan hepatocyte-specific T1 contrast agent for MRI, Biomaterials 32 (2011) 5187–5194.
[3] K.S. Kim, W. Park, J. Hu, Y.H. Bae, K. Na, A cancer-recognizable MRI contrast agents using pH-responsive polymeric micelle, Biomaterials 35 (2014) 337–343.
[4] X.H. Ma, A. Gong, L.C. Xiang, T.X. Chen, Y.X. Gao, X.J. Liang, Z.Y. Shen, A.G. Wu, Biocompatible composite nanoparticles with large longitudinal relaxivity for targeted imaging and early diagnosis of cancer, J. Mater. Chem. B 1 (2013) 3419–3428.
[5] X. Ma, A. Gong, B. Chen, J. Zheng, T. Chen, Z. Shen, A. Wu, Exploring a new SPION-based MRI contrast agent with excellent water-dispersibility, high specificity to cancer cells and strong MR imaging efficacy, Colloid Surf. B 126 (2015) 44–49.
[6] H. Xie, Y. Zhu, W. Jiang, Q. Zhou, H. Yang, N. Gu, Y. Zhang, H. Xu, H. Xu, X. Yang, Lactoferrin-conjugated superparamagnetic iron oxide nanoparticles as a specific MRI contrast agent for detection of brain glioma in vivo, Biomaterials 32 (2011) 495–502.
[7] Q. Zhang, X. Wang, P.Z. Li, K.T. Nguyen, X.J. Wang, Z. Luo, H. Zhang, N.S. Tan, Y. Zhao, Biocompatible, uniform, and redispersible mesoporous silica nanoparticles for cancer-targeted drug delivery in vivo, Adv. Funct. Mater. 24 (2014) 2450–2461.
[8] J. Xie, Y. Zhang, C. Yan, L. Song, S. Wen, F. Zang, G. Chen, Q. Ding, C. Yan, N. Gu, High-performance PEGylated Mn-Zn ferrite nanocrystals as a passive-targeted agent for magnetically induced cancer theranostics, Biomaterials 35 (2014) 9126–9136.
[9] G. Chen, L. Wang, T. Cordie, C. Vokoun, K.W. Eliceiri, S. Gong, Multi-functional self-fluorescent unimolecular micelles for tumor-targeted drug delivery and bioimaging, Biomaterials 47 (2015) 41–50.
[10] D. Peer, J.M. Karp, S. Hong, O.C. Farokhzad, R. Margalit, R. Langer, Nanocarriers as an emerging platform for cancer therapy, Nat. Nanotechnol. 2 (2007) 751–760.
[11] D.M. Copolovici, K. Langel, E. Eriste, U. Langel, Cell-penetrating peptides: design, synthesis, and applications, ACS Nano 8 (2014) 1972–1994.
[12] L. Jiang, L. Li, X. He, Q. Yi, B. He, J. Cao, W. Pan, Z. Gu, Overcoming drug-resistant lung cancer by paclitaxel loaded dual-functional liposomes with mitochondria targeting and pH-response, Biomaterials 52 (2015) 126–139.
[13] A. Schroeder, D.A. Heller, M.M. Winslow, J.E. Dahlman, G.W. Pratt, R. Langer, T. Jacks, D.G. Anderson, Treating metastatic cancer with nanotechnology, Nat. Rev. Cancer 12 (2012) 39–50.
[14] X.B. Xiong, A. Lavasanifar, Traceable multifunctional micellar nanocarriers for cancer-targeted co-delivery of MDR-1 siRNA and doxorubicin, ACS Nano 5 (2011) 5202–5213.
[15] M. Muthiah, H. Vu-Quang, Y.K. Kim, J.H. Rhee, S.H. Kang, S.Y. Jun, Y.J. Choi, Y.Y. Jeong, C.S. Cho, I.K. Park, Mannose-poly(ethylene glycol)-linked SPION targeted to antigen presenting cells for magnetic resonance imaging on lymph node, Carbohyd. Polym. 92 (2013) 1586–1595.
[16] J.H. Maeng, D.H. Lee, K.H. Jung, Y.H. Bae, I.S. Park, S. Jeong, Y.S. Jeon, C.K. Shim,

W. Kim, J. Kim, J. Lee, Y.M. Lee, J.H. Kim, W.H. Kim, S.S. Hong, Multifunctional doxorubicin loaded superparamagnetic iron oxide nanoparticles for chemotherapy and magnetic resonance imaging in liver cancer, Biomaterials 31 (2010) 4995–5006.
[17] J. Nam, N. Won, H. Jin, H. Chung, S. Kim, pH-induced aggregation of gold nanoparticles for photothermal cancer therapy, J. Am. Chem. Soc. 131 (2009) 13639–13645.
[18] Y. Bae, N. Nishiyama, S. Fukushima, H. Koyama, M. Yasuhiro, K. Kataoka, Preparation and biological characterization of polymeric micelle drug carriers with intracellular pH-triggered drug release property: tumor permeability, controlled subcellular drug distribution, and enhanced in vivo antitumor efficacy, Bioconjugate Chem. 16 (2005) 122–130.
[19] M. Hruby, C. Konak, K. Ulbrich, Polymeric micellar pH-sensitive drug delivery system for doxorubicin, J. Control Release 103 (2005) 137–148.
[20] X. Yin, A.S. Hoffman, P.S. Stayton, Poly(N-isopropylacrylamide-co-propylacrylic acid) copolymers that respond sharply to temperature and pH, Biomacromolecules 7 (2006) 1381–1385.
[21] A.J. Convertine, N. Ayres, C.W. Scales, A.B. Lowe, C.L. McCormick, Facile, controlled, room-temperature RAFT polymerization of N-isopropylacrylamide, Biomacromolecules 5 (2004) 1177–1180.
[22] J. Zhang, N.A. Peppas, Synthesis and characterization of pH- and temperature-sensitive poly(methacrylic acid)/poly(N-isopropylacrylamide) interpenetrating polymeric networks, Macromolecules 33 (2000) 102–107.
[23] Q. Xu, W. Huang, L. Jiang, Z. Lei, X. Li, H. Deng, KGM and PMAA based pH-sensitive interpenetrating polymer network hydrogel for controlled drug release, Carbohyd. Polym. 97 (2013) 565–570.
[24] Z. Shen, K. Terao, Y. Maki, T. Dobashi, G. Ma, T. Yamamoto, Synthesis and phase behavior of aqueous poly(N-isopropylacrylamide-co-acrylamide), poly(N-isopropylacrylamide-co-N,N-dimethylacrylamide) and poly(N-isopropylacrylamide-co-2-hydroxylethyl methacrylate), Colloid Polym. Sci. 284 (2006) 1001–1007.
[25] N. Lu, J. Liu, J. Li, Z. Zhang, Y. Weng, B. Yuan, K. Yang, Y. Ma, Tunable dual-stimuli response of a microgel composite consisting of reduced graphene oxide nanoparticles and poly(N-isopropylacrylamide) hydrogel microspheres, J. Mater. Chem. B 2 (2014) 3791–3798.
[26] J. Dong, J. Weng, L. Dai, The effect of graphene on the lower critical solution temperature of poly(N-isopropylacrylamide), Carbon 52 (2013) 326–336.
[27] Z. Shen, B. Shi, H. Zhang, J. Bi, S. Dai, Exploring low-positively-charged thermosensitive copolymers as gene delivery vectors, Soft Matter 8 (2012) 1385–1394.
[28] H.L. Ma, X.R. Qi, Y. Maitani, T. Nagai, Preparation and characterization of superparamagnetic iron oxide nanoparticles stabilized by alginate, Int. J. Pharm. 333 (2007) 177–186.
[29] R.K. Gosavi, U. Agarwala, C.N.R. Rao, Infrared spectra and configuration of alkylthiourea derivatives. Normal vibrations of N,N′-dimethyl- and tetramethylthiourea, J. Am. Chem. Soc. 89 (1967) 235–239.
[30] Z. Shen, W. Wei, G. Ma, Y. Zhao, T. Dobashi, Y. Maki, S. Su, J. Wan, Thermosensitive polymer-conjugated albumin nanospheres as thermal targeting anticancer drug carrier, Eur. J. Pharm. Sci. 35 (2008) 271–282.
[31] Z. Shen, W. Wei, H. Tanaka, K. Kohama, G. Ma, T. Dobashi, Y. Maki, H. Wang, J. Bi, S. Dai, A galactosamine-mediated drug delivery carrier for targeted liver cancer therapy, Pharmacol. Res. 64 (2011) 410–419.
[32] P.R. Gil, D.J.D. Aberasturi, V. Wulf, B. Pelaz, P.D. Pino, Y. Zhao, J.M.D.L. Fuente, I.R.D. Larramendi, T. Rojo, X.J. Liang, W.J. Parak, The challenge to relate the physicochemical properties of colloidal nanoparticles to their cytotoxicity, Acc. Chem. Res. 46 (2013) 743–749.
[33] S. Huang, Y. Wan, Z. Wang, J. Wu, Folate-conjugated chitosan-polylactide nanoparticles for enhanced intracellular uptake of anticancer drug, J. Nanopart. Res. 15 (2013) 2096.
[34] J. Chen, S. Li, Q. Shen, Folic acid and cell-penetrating peptide conjugated PLGA-PEG bifunctional nanoparticles for vincristine sulfate delivery, Eur. J. Pharm. Sci. 47 (2012) 430–443.
[35] X.Z. Sheng, Z.Q. Liu, L.B. Wu, J. Tang, C.R. Zhao, L.B. Kong, Q. Wang, C.D. Wang, Technical feasibility and histopathologic studies of poly(N-isopropylacrylamide) as a non-adhesive embolic agent in swine rete mirabile, Chin. Med. J. 119 (2006) 391–396.